Brain Connectivity

DOI: 10.1089/brain.2016.0435

Title: Evaluation of Denoising Strategies To Address Motion-Correlated Artifact in Resting State fMRI Data from the Human Connectome Project

Authors: Gregory C. Burgess[1] (gburgess@wustl.edu), Sridhar Kandala[2] (kandalas@wustl.edu), Dan Nolan[2] (dhnolan@wustl.edu), Timothy O. Laumann[3] (laumannt@wustl.edu), Jonathan D. Power[4] (jonathan.power@nih.gov), Babatunde Adeyemo[3] (badeyemo@wustl.edu), Michael P. Harms[2] (mharms@wustl.edu), Steven E. Petersen[1,3,5,6] (sep@wustl.edu), Deanna M. Barch[2,5,6] (dbarch@wustl.edu)

Author Affiliations:
Departments of Neuroscience[1], Psychiatry[2], Neurology[3], Radiology[5]; Washington University School of Medicine; St. Louis, MO 63110 USA
National Institute of Mental Health[4]; Bethesda, MD 20892 USA
Department of Psychology[6]; Washington University in St. Louis; St. Louis, MO 63130 USA

Corresponding Author:
Gregory C. Burgess
Department of Neuroscience
Washington University School of Medicine
Campus Box 8225
St. Louis, MO 63110-1093
email: gburgess@wustl.edu
phone: 314-362-7864
fax: 314-362-3392

Running Title: Motion-Correlated Artifact in HCP rfMRI Data

Keywords: fMRI, Motion, Artifact, Denoising, Resting state, Functional connectivity, Human Connectome Project, Independent Component Analysis

Brain Connectivity
Evaluation of Denoising Strategies To Address Motion-Correlated Artifact in Resting State fMRI Data from the Human Connectome Project (doi: 10.1089/brain.2016.0435)
This paper has been peer-reviewed and accepted for publication, but has yet to undergo copyediting and proof correction. The final published version may differ from this proof.

Abstract

Like all resting-state functional connectivity data, the data from the Human Connectome Project (HCP) are adversely affected by structured noise artifact arising from head motion and physiological processes. Functional connectivity estimates (Pearson's correlation coefficients) were inflated for high-motion time points and for high-motion participants. This inflation occurred across the brain, suggesting the presence of globally-distributed artifact. The degree of inflation was further increased for connections between nearby regions compared to distant regions, suggesting the presence of distance-dependent, spatially-specific artifact. We evaluated several denoising methods: censoring high-motion time points, motion regression, FMRIB's ICA-based X-noiseifier (FIX), and mean grayordinate time series regression (MGTR; as a proxy for global signal regression). The results suggest that FIX-denoising reduced both types of artifact, but left substantial global artifact behind. MGTR significantly reduced global artifact, but left substantial spatially-specific artifact behind. Censoring high-motion time points resulted in a small reduction of distance-dependent and global artifact, eliminating neither type. All denoising strategies left differences between high- and low-motion participants, but only MGTR substantially reduced those differences. Ultimately, functional connectivity estimates from HCP data showed spatially-specific and globally-distributed artifact, and the most effective approach to address both types of motion-correlated artifact was a combination of FIX and MGTR.

Acronyms

BOLD:	blood oxygen level dependent
CIFTI:	Connectivity Informatics Technology Initiative
DVARS:	temporal Derivative, then RMS VARiance over elementS
FD:	Framewise Displacement
FIX:	FMRIB's ICA-based X-noiseifier
HCP:	Human Connectome Project
ICA:	Independent Component Analysis
MGTR:	mean grayordinate time series regression
MPP:	minimally preprocessed
pCO_2:	partial pressure of carbon dioxide in blood
QC:	quality control
rfMRI:	resting-state functional magnetic resonance imaging
rsFC:	resting state functional connectivity

Introduction

The Human Connectome Project (HCP) endeavors to reveal variations in connectivity and their relation to behavior, function, and genetics in 1200 healthy participants (Van Essen et al., 2013). HCP advanced cutting-edge pulse sequences to provide resting-state functional magnetic resonance imaging (rfMRI) data with high spatial and temporal resolution and whole-brain coverage (Ugurbil et al., 2013). Nonetheless, HCP rfMRI data, like most rfMRI data, are likely contaminated by artifact resulting from a number of influences, including head motion, scanner-related issues, and physiological processes related to cardiac, respiratory, and pCO_2 fluctuations. The intention of the current work was to focus on artifact correlated with head motion and the effectiveness of methods designed to reduce such artifacts.

Motion-correlated artifact can bias our understanding of functional networks and their relationship with individual- and group-difference variables (Power et al., 2012; Van Dijk et al., 2012; Yan et al., 2013b). Prior studies using lower-resolution rfMRI data provided approaches to address motion-correlated artifact (Jo et al., 2013; Muschelli et al., 2014; Satterthwaite et al., 2013), reviewed in Power (2015). These denoising strategies demonstrated varying degrees of efficacy, but it is unclear whether they will benefit higher-resolution HCP rfMRI data to the same degree.

Indicators Suggestive of Motion-Correlated Artifact

In this paper, we took four approaches to interrogating the relationship between head motion and artifact in rfMRI data (c.f., Power et al., 2014): (i) intensity fluctuations in time series data, (ii) distance-dependent artifacts, (iii) elevated differences between

low- and high-motion groups, and (iv) relationships between head motion and resting state functional connectivity (rsFC) estimates. As in the existing literature, we expect motion-correlated artifact to take two forms: global effects and spatially-specific or distance-dependent effects.

(i) Fluctuations in time series data: Power and colleagues (2014; 2012) demonstrated that modest movements of the head are associated with large blood oxygen level dependent (BOLD) signal changes across gray matter, white matter, and cerebrospinal fluid voxels. Motion-correlated fluctuations in BOLD signal appear quite complex: they may increase, decrease, or both before returning to baseline; they may fluctuate across the whole brain (i.e., globally-distributed), and in some regions more than others (i.e., spatially-specific); and they may be brief (Satterthwaite et al., 2013) or temporally-extended (10 or more seconds after motion ends, Power et al., 2014). Some of these BOLD fluctuations may directly result from motion, and others may be motion-correlated artifact due to physiological processes time-locked to motion (e.g., yawning moves the head, but also changes heart rate and pCO_2 concentration). Either way, the concern is that motion-correlated artifact influences rfMRI data for all individuals on average, but more for high-motion than low-motion individuals.

(ii) Distance-dependent artifact: Artifactual variance during motion tends to be more similar for nearby voxels than distant voxels (see discussion in Power et al., 2015). This results in correlations between head motion and rsFC estimates that are higher for short-distance connections and lower for long-distance connections (Satterthwaite et al., 2012). Censoring (i.e., removing) high-motion time points reduces

motion-correlated artifact and usually decreases correlations between nearby parcels and increases correlations between more-distant parcels (Power et al., 2014; 2012).

(iii) Motion-group differences: Head motion during rfMRI scans varies across individuals, and may be confounded with factors of interest, such as age (Power et al., 2012), attention deficit hyperactivity disorder and impulsivity (Epstein et al., 2007; Kong et al., 2014), and bipolar disorder and schizophrenia (Mamah et al., 2013). Unfortunately, rsFC estimates also appear biased in higher-motion versus lower-motion individuals and groups (Van Dijk et al., 2012). Differences between groups that vary in head motion are apparent across the frequency spectrum (Satterthwaite et al., 2013) and across analysis strategies (Power et al., 2015; Satterthwaite et al., 2012; Yan et al., 2013b).

(iv) QC-rsFC plots: The relationship between individual differences in head motion and rsFC estimates can also be interrogated with QC-rsFC plots: plots of the correlation across participants between quality control (QC) measures of head motion during the scan and rsFC estimates. Previous investigations using QC-rsFC plots (Muschelli et al., 2014; Power et al., 2014; Satterthwaite et al., 2013) show higher rsFC estimates in individuals with greater head motion. These increased rsFC estimates exist across the whole brain (i.e., global) but to a greater extent for short-distance connections (i.e., spatially-specific). Although methods such as aCompCor (Muschelli et al., 2014) and censoring (Power et al., 2014) reduce spatially-specific effects, they fail to substantially reduce global effects.

Goals of the current study

Here, we investigate the relationship between estimated head motion and resting state correlations in HCP data. Using the procedures of Power and colleagues (2014),

Evaluation of Denoising Strategies To Address Motion-Correlated Artifact in Resting State fMRI Data from the Human Connectome Project (doi: 10.1089/brain.2016.0435)
This paper has been peer-reviewed and accepted for publication, but has yet to undergo copyediting and proof correction. The final published version may differ from this proof.

Brain Connectivity

we investigate BOLD fluctuations and distance-dependent changes in correlations related to high-motion time points, and report how group- and individual-differences in head motion relate to differences in rsFC estimates. We investigated the efficacy of several denoising techniques including: motion regression, censoring of high-motion time points, FIX-denoising, and MGTR (see Methods section "*Mean grayordinate time series regression" for more information)*.

Materials and Methods

Participants:

This investigation evaluated rfMRI data from the HCP "500 Subjects" Public Data Release. HCP participants were between 22 and 35 years of age at the time of recruitment, and did not have a documented history of psychiatric, neurological, or medical disorders known to influence brain function. For a more-detailed description of inclusion and exclusion criteria for HCP, see Van Essen and colleagues (2013).

The sample of participants included 183 participants (mean age = 29.11, sd = 3.55), divided into three motion-groups with 26 men and 35 women in each. (Information about demographics and motion are presented in Table 1. See "Selecting motion-groups" in the Supplement for more details.) The three motion groups did not differ with respect to age [$F(2,180) = 0.37$, $p = 0.693$], years of education [$F(2,178) = 1.35$, $p = 0.263$], race [$\chi^2(8) = 3.79$, $p = 0.878$], or ethnicity [$\chi^2(2) = 2.26$, $p = 0.323$]. By design, the motion groups did differ with respect to the proportion of high-motion time points in their scans [$F(2,180) = 232.79$, $p = 1.20 \times 10^{-50}$] and mean FD [$F(2,180) = 66.17$, $p = 3.06 \times 10^{-22}$].

Image acquisition:

Details of the MRI acquisition parameters for the HCP were described elsewhere (Ugurbil et al., 2013). Structural T1-weighted and T2-weighted images were collected at 0.7 mm isotropic resolution. Whole-brain EPI acquisitions were acquired on the 3T Siemens Connectom scanner: 32-channel head coil, TR = 720 ms, TE = 33.1 ms, in-plane FOV = 208 x 180 mm, 72 slices, 2.0 mm isotropic voxels, multi-band acceleration factor of 8 (Feinberg et al., 2010).

Brain Connectivity
Evaluation of Denoising Strategies To Address Motion-Correlated Artifact in Resting State fMRI Data from the Human Connectome Project (doi: 10.1089/brain.2016.0435)
This paper has been peer-reviewed and accepted for publication, but has yet to undergo copyediting and proof correction. The final published version may differ from this proof.

Overview of four types of preprocessed rfMRI data:

We evaluated the reduction in motion-correlated artifact after FIX-denoising (e.g., removing variance classified as noise by FIX) versus without FIX-denoising, and after MGTR versus without MGTR. Crossing these two factors of interest yielded four types of preprocessed rfMRI data: FIX, MPP, FIX+MGTR, MPP+MGTR.

Preprocessing of HCP rfMRI data

The HCP FIX-denoising pipeline uses a gentle high-pass temporal filter (using 'fslmaths' with 2000 second cutoff), motion regression (i.e., regression of 24 movement parameters: six rigid-body motion parameters, their backward temporal derivatives, and squares of those twelve time series), and applies a "non-aggressive" regression based on independent component analysis (ICA) to remove variance in noise components that was orthogonal to signal components (Salimi-Khorshidi et al., 2014).

The inputs to our preprocessing stream were both minimally-preprocessed (MPP) and FIX-denoised rfMRI data from the HCP 500 subject release. To ensure that comparisons between MPP and FIX-denoised data primarily reflected differences due to "non-aggressive" regression of ICA noise components, we preprocessed the MPP data using procedures similar to the FIX-denoising pipeline, including the lenient high-pass temporal filter (2000 second cutoff) and motion regression but excluding the regression of ICA noise component variance. Additional high-pass filtering (0.009 Hz) was conducted after regressing these confound time series (Carp, 2013). (Additional details about the *HCP Minimal Preprocessing Procedures* and *HCP FIX-Denoising Procedures* are provided in Supplemental Materials.)

Mean grayordinate time series regression

Our analyses utilized the CIFTI dense time series files, which represent the rfMRI time series for 91282 "grayordinates" (i.e., surface-based vertices and subcortical voxels, constrained to gray matter; see Glasser et al., 2013 for more details about CIFTI format). Therefore, rather than global signal regression, we performed mean grayordinate time series regression (MGTR): computing the mean grayordinate time series from the MPP or FIX data, then regressing it and its backward derivative from each grayordinate. Although the mean grayordinate time series reflects gray matter only, MGTR seems a reasonable replacement for global signal regression due to the strong average correlation between the global signal and mean grayordinate time series (r=0.94).

Using Grayordinate Plots to Visualize Fluctuations in rfMRI Data:

"Residual grayordinate plots" (shown in grayscale) display the time series after denoising. These reflect the nature of rfMRI data going into rsFC estimation after each denoising strategy. "Difference grayordinate plots" (shown in color) reflect BOLD fluctuations removed by each denoising strategy, computed as the difference between the current stage and a specified previous stage.

Both types of grayordinate plots display the time series data across time points (columns) and grayordinates (rows). Intensities are displayed as z-scores, standardized relative to the mean and standard deviation for that grayordinate. White or black values in the "residual grayordinate plots" and red or blue values in the "difference grayordinate plots" reflect time points when the BOLD signal for that grayordinate is relatively extreme (greater than 2 standard deviations from the mean). These values might influence correlation values strongly.

Censoring, and its role in identifying motion-correlated artifact:

In analyses involving censoring, we explicitly deleted high-motion time points from the time series prior to analysis. High-motion time points were identified using a combination of FD and DVARS thresholds (as defined in Supplemental section "*Defining high-motion time points – FD and DVARS*"), were defined from the original MPP data, and were identical for each denoising strategy.

We censored high-motion time points not only as a strategy to reduce motion-correlated artifact, but also as a means to index any remaining artifact still correlated with head motion. Previous evaluations showed changes in rsFC estimates after censoring high-motion time points (Power et al., 2014; 2012; Yan et al., 2013b; 2013a). If motion-correlated artifact is present, high-motion time points will distort rsFC estimates. If denoising removes motion-correlated artifact entirely, then rsFC estimates involving high-motion time points will no longer be distorted, and will not differ from rsFC estimates involving only low-motion time points. Therefore, comparing rsFC estimates for censored data (i.e., low-motion time points only) to rsFC estimates for uncensored data (i.e., low-motion and high-motion time points) will identify motion-correlated artifact remaining after each denoising strategy.

Parcellated connectomes:

Functional connectivity was evaluated in subsequent analyses using full correlations (Pearson's correlation coefficients) between parcel time series extracted from CIFTI grayordinates. We utilized the 333 cortical parcels from the Gordon and colleagues (2014) parcellation because they have higher functional homogeneity than several other published parcellation schemes. We also added 19 subcortical parcels

from the group-average CIFTI atlas, for a total of 352 parcels. (Additional detail about *Parcellated Connectomes* is included in Supplemental Materials.)

ΔR plots Display Motion-Correlated Artifact from High-Motion Time Points:

The influence of residual motion-correlated artifact may be revealed with ΔR plots – i.e., the difference between rsFC estimates derived from censored versus uncensored data. For each connection, rsFC estimates are computed using the censored time series, and the uncensored time series. RSFC estimates are Fisher z-transformed, averaged across participants, and converted back to Pearson's r. The difference between rsFC estimates (averaged across participants) from censored and uncensored data is then plotted as a function of the distance between parcels.

The slope of these ΔR plots may demonstrate distance-dependent effects, indicating that residual motion-correlated artifact differs for short-distance versus long-distance connections. A shift in the mean of the ΔR plots may indicate global influences on rsFC estimates, such that high-motion time points increase correlations across all connections regardless of distance.

The mean ΔR and the linear relationship of ΔR with distance from a general linear model (GLM) will estimate the global and distance-dependent effects, respectively. However, because each parcel contributes to multiple rsFC observations, rsFC observations are non-independent. Statistical inference on the mean and slope is biased by non-independent observations. However, the parameter estimates themselves are unbiased. After accounting or controlling for family structure, participants provide independent observations to conduct valid statistical inference.

Therefore, we fit a GLM for each participant, predicting ΔR with an intercept term and a distance term (i.e, Euclidean distance between parcels, after mean-centering). This yielded independent observations of the mean and slope. Then, one-sample t-tests determined whether those parameters were different from zero in the high-motion group (Table 2) and in the low-motion group (Table S1).

To estimate differences between two denoising strategies, we computed the difference in ΔR values between two strategies, then predicted those values using a GLM for each participant with intercept and distance terms. The mean and slope reflected the difference in global and distance-dependent effects between the two strategies. Finally, one-sample t-tests across high-motion (Table 2) and low-motion (Table S1) participants indicated whether the means and slopes differed from zero.

QC-rsFC plots reveal residual distance-dependent and global artifact after censoring:

For each pairwise connection, correlations were computed across 183 participants between the value of the rsFC estimate (after censoring) and the proportion of time points censored under the combined FD and DVARS criteria. These QC-rsFC correlations were plotted as a function of distance between the regions to examine whether distance-dependent artifact might be present in the rfMRI time series. At the same time, QC-rsFC correlations that are elevated across all distances are suggestive of global artifact remaining in the time series.

To determine the statistical significance of global and distance-dependent effects in the QC-rsFC plots, we used a similar approach to significance testing of the ΔR plots. First, for each participant, a GLM predicted rsFC estimates with intercept and distance terms, providing independent estimates of the global (mean) and distance-

dependent (slope) effects. Second, to determine if individual differences in head motion modulated global and distance-dependent effects, group-level GLMs predicted the subject-level parameters with a "QC" term (i.e., head motion estimated by proportion of time points censored, after mean-centering) and an intercept. We estimated the significance of the global QC-rsFC relationship by "QC" predicting the mean, and the significance of the distance-dependent QC-rsFC relationship by "QC" predicting the slope. We report these results separately for censored data (Table 3) and uncensored data (Table S2).

To estimate differences between denoising strategies, we computed the difference in rsFC values between two strategies, then predicted those values for each participant using a GLM with intercept and distance terms. The mean and slope reflect the difference in global and distance-dependent effects between those two strategies. Then, we estimated whether those parameters related to the degree of head motion ("QC") across participants.

Computing motion-group differences:

We computed the percentage of significant "motion-group differences" observed in the correlation matrices after each denoising strategy. For a given rsFC estimate, unpaired t-tests determined whether motion-group differences (e.g., between high- and low-motion groups) were significant. (See "*Establishing alpha level for testing motion-group differences" in the Supplement for more details.)* We reported the percentage of significant motion-group differences across all connections, and separately for short-distance (4.8 mm – 58.6 mm), medium-distance (58.6 mm – 112.3 mm), and long-distance (112.3 mm – 166.1 mm) connections.

Evaluation of Denoising Strategies To Address Motion-Correlated Artifact in Resting State fMRI Data from the Human Connectome Project (doi: 10.1089/brain.2016.0435)
This paper has been peer-reviewed and accepted for publication, but has yet to undergo copyediting and proof correction. The final published version may differ from this proof.

Brain Connectivity

For each denoising strategy, we used permutation testing to determine whether the observed number of motion-group differences was significantly greater than expected by chance. The null distribution was estimated by permuting motion-group labels across participants 10000 times.

Results

Grayordinate plots display spatially-specific and global fluctuations

Figure 1 shows grayordinate plots from HCP participant 107422 from time points 600 - 1000 (4.8 minutes) of their rfMRI_REST1_RL scan. This participant had below-average head motion, but features evident in these data are present across the full sample of HCP participants.

----------Insert Figure 1 about here----------

Global and spatially-specific artifact is evident in HCP MPP rfMRI data prior to motion regression. The residual grayordinate plot (Figure 1A) prominently displays global fluctuations as vertical bands that show similar sign (i.e., positive or negative) and magnitude across most grayordinates. Some example time periods are indicated by green arrows. Global fluctuations vary in duration, with some lasting 20 seconds or more. Spatially-specific fluctuations appear as horizontal bands that varied in sign and magnitude across grayordinates. Some examples are indicated by red and blue arrows.

Spatially-Specific Artifact is Reduced by Motion Regression and FIX-denoising: In some cases, spatially-specific noise was isolated to a small proportion of grayordinates but extended over several time points. These manifest as rows of higher or lower intensity (red arrows in Figure 1A). These are reduced by motion regression (red arrow in Figure 1F) and FIX-denoising (red arrows in Figure 1G), resulting in reduced noise in the residual grayordinate plots (red arrows in Figure 1B and 1C). In other cases, spatially-specific artifact was evident at specific time points, but showed effects that varied in sign and magnitude across grayordinates. This spatially-specific artifact is evident in the variance removed by motion regression (Figure 1F blue arrows)

and FIX-denoising (Figure 1G blue arrows). Despite the artifact removed by these strategies, the residual grayordinate plots show clear global fluctuations left behind by both motion regression (Figure 1B) and FIX-denoising (Figure 1C).

Global Fluctuations are Slightly Reduced by FIX-Denoising, but Dramatically Reduced by MGTR: FIX-denoising appeared to target some time points that exhibit global fluctuations (Figure 1G green arrows). Some of these global fluctuations occurred after spikes in DVARS or FD, but others did not. FIX-denoising results in a reduction in the magnitude of global fluctuations, but FIX rfMRI data still show substantial global fluctuations (Figure 1C green arrows) in the grayordinate time series. However, MGTR dramatically reduced or eliminated the global fluctuations (Figures 1D and 1H).

Combining FIX-denoising and MGTR reduced both spatially-specific and global fluctuations: The above results suggest that FIX-denoising and MGTR have different types of effects on motion-correlated fluctuations in the rfMRI data. The differences are most easily observed in the difference grayordinate plots, where it appears that combining FIX-denoising and MGTR controls *both* spatially-specific fluctuations and global fluctuations in those data (Figure 1J).

ΔR Plots reveal distance-dependent and global artifact

Within the high-motion group, ΔR plots show both distance-dependent (spatially-specific) and global artifact. Censoring high-motion time points elucidates distance-dependent artifact present in MPP rfMRI data (Figure 2A), confirmed by a statistically significant slope as a function of distance (Table 2). In the FIX rfMRI data (Figure 2B), censoring appears to reduce both global and distance-dependent artifact, as indicated by a statistically significant mean and slope related to distance (Table 2). The reduction

in distance-dependent artifact due to censoring is visually evident in ΔR plots from MPP+MGTR and FIX+MGTR data (Figure 2C and 2D). However, both the mean and slope of the ΔR effect were statistically different from zero in MPP+MGTR and FIX+MGTR data (Table 2).

----------Insert Figure 2 about here----------

----------Insert Table 2 about here----------

We evaluated differences in ΔR between denoising strategies to determine whether those denoising strategies might reduce distance-dependent and global artifact. Neither the difference between FIX and MPP rfMRI data nor the difference between MPP+MGTR and MPP rfMRI data showed significant distance-dependent or global ΔR effects (Table 2). One might assume that this indicates that neither denoising strategy removes motion-correlated artifact. However, the high variability of the MPP rfMRI data might have reduced our sensitivity to the effects of FIX and MGTR. Consistent with this hypothesis, the difference between FIX+MGTR and FIX rfMRI data is significant for the mean term, and the difference between FIX+MGTR and MPP+MGTR is significant for both the mean and slope. These findings are consistent with our interpretation of the grayordinate plots: that MGTR reduces global fluctuations, and that FIX reduces spatially-specific fluctuations as well as global fluctuations. The results were similar for low-motion participants (Supplemental Figure S3 and Supplemental Table S1).

QC-rsFC plots reveal residual distance-dependent and global artifact after censoring:

We investigated the relationship between rsFC estimates and individual differences in estimated head motion (Figure 3 and Table 3). The MPP rfMRI data

Brain Connectivity
Evaluation of Denoising Strategies To Address Motion-Correlated Artifact in Resting State fMRI Data from the Human Connectome Project (doi: 10.1089/brain.2016.0435)
This paper has been peer-reviewed and accepted for publication, but has yet to undergo copyediting and proof correction. The final published version may differ from this proof.

shows both global and distance-dependent relationships between rsFC estimates and the amount of motion during the scan, even after censoring, supported by the fact that head motion is significantly related to both the mean and slope as a function of distance. FIX-denoising resulted in a statistically significant reduction in the relationship of head motion with the mean, but head motion still modulated both the mean and slope in FIX data. MPP+MGTR data showed a larger reduction in the relationship between head motion and the mean compared to MPP data, but again head motion still modulated both the mean and slope in MPP+MGTR data. For FIX+MGTR data (after censoring) the global relationship with head motion was still statistically significant, albeit at its lowest level, but the distance-dependent relationship with head motion was eliminated. Global and distance-dependent effects were significantly reduced in FIX+MGTR data relative to both FIX data and MPP+MGTR data. These effects were similar for uncensored data (Supplemental Figure S4 and Supplemental Table S2).

----------Insert Figure 3 about here----------

----------Insert Table 3 about here----------

Substantial differences exist between motion groups, and are primarily reduced by MGTR:

Consistent with prior work (Power et al., 2014), the observed number of differences between the low- and high-motion groups was inflated strongly above chance in the MPP rfMRI data (Table 4). Both censoring high-motion time points and FIX-denoising reduced the number of motion-group differences slightly, but the number of motion-group differences was still substantially elevated. In contrast, MGTR

dramatically reduced the number of differences between high- and low-motion groups, albeit not to chance levels, for both MPP+MGTR and FIX+MGTR rfMRI data.

----------Insert Table 4 about here----------

Discussion

The current study evaluated the presence of motion-correlated artifact in HCP rfMRI data and its removal by some common denoising strategies. Consistent with prior work (Power et al., 2014; 2012; Satterthwaite et al., 2013; Van Dijk et al., 2012), the current results suggest two separate classes of motion-correlated artifact: global and spatially-specific. The denoising strategies we tested differed in efficacy for these two classes. Consequently, a combination of methods – such as FIX-denoising to reduce spatially-specific artifact and MGTR to reduce global artifact – will be necessary to effectively address motion-corrected artifact.

Denoising strategies had differential effects on motion-correlated artifact

Motion regression, censoring, and FIX-denoising seemed to have the largest effect on spatially-specific artifact. The grayordinate plots revealed that motion regression strongly affected some grayordinates but affected others not at all, and the sign of the effect varied across grayordinates. Censoring high-motion time points demonstrated a distance-dependent reduction in the ΔR plot for MPP rfMRI data. FIX reduced distance-dependent artifact, as indexed by the comparison of FIX+MGTR versus MPP+MGTR data in the ΔR and QC-rsFC plots.

On the other hand, evidence of global artifact was only reduced substantially by MGTR. Global artifact manifested as vertical bands in residual grayordinate plots, influences of high-motion time points across all distances in ΔR plots, and relationships between motion estimates and rsFC estimates across the entire brain in QC-rsFC plots. These global effects were significantly reduced for FIX+MGTR data compared to FIX data.

Evaluation of Denoising Strategies To Address Motion-Correlated Artifact in Resting State fMRI Data from the Human Connectome Project (doi: 10.1089/brain.2016.0435)
This paper has been peer-reviewed and accepted for publication, but has yet to undergo copyediting and proof correction. The final published version may differ from this proof.

Motion-group differences were reduced by FIX and by censoring. However, these reductions were relatively modest. They did not appear more strongly for short-distance connections, as might be expected from a reduction in spatially-specific artifact. In contrast, MGTR reduced motion-group differences substantially across all distance bins. This pattern suggests that the bulk of motion-group differences resulted from globally-distributed artifact, as opposed to spatially-specific artifact.

FIX-denoising seems to primarily address spatially-specific artifact while doing less to address global artifact. Perhaps that should not be surprising. First, as with many other ICA-based denoising methods, FIX-denoising uses spatial ICA algorithms that maximize the spatial independence of components. Consequently, global noise variance is less likely to be isolated into a separate component and removed by ICA-denoising. Temporal ICA algorithms may be more likely to identify global components (Smith et al., 2012), which subsequently might be classified as noise. Second, the HCP FIX-ICA denoising pipeline applies “non-aggressive” denoising, regressing only the portion of noise variance orthogonal to signal components. Non-aggressive denoising may not remove global noise that is shared across signal and noise components (Smith et al., 2013).

Censoring appears to reduce spatially-specific artifact. However, the significant slope of the QC-rsFC relationship for MPP and MPP+MGTR data suggests that censoring did not eliminate distance-dependent artifact as reported in previous studies. We postulate that the reduced efficacy of the censoring procedure in HCP rfMRI data might result in part from increased noise variance in the FD and DVARS motion estimates, as discussed in the *Supplemental Materials*.

Brain Connectivity
Evaluation of Denoising Strategies To Address Motion-Correlated Artifact in Resting State fMRI Data from the Human Connectome Project (doi: 10.1089/brain.2016.0435)
This paper has been peer-reviewed and accepted for publication, but has yet to undergo copyediting and proof correction. The final published version may differ from this proof.

Potential influences of physiological noise in HCP rfMRI data

The rfMRI time series from many HCP participants contain periodic fluctuations in signal intensity across the brain. These are visible as evenly-spaced global bands in the grayordinate plots, resulting in periodic fluctuations in the mean grayordinate time series (cf., center of Figure 1A). One intriguing question is whether some portion of this motion-correlated global artifact might be physiological in origin. Head motion and physiological artifact may be coupled if respiratory movements directly cause head motion (e.g., yawning, sneezing, deep breathing or sighing), if ballistocardiographic forces directly cause head motion, or if effort exerted while moving the head and body in the scanner results in breath holding or change in heart rate.

Interestingly, the global artifact in HCP rfMRI data (Figure 1A) and other rfMRI data (Power et al., 2014) seems to lag head motion by 10 – 20 seconds. It has also been shown that respiratory artifact has a response function that extends across a similar time frame (Birn et al., 2008; Chang and Glover, 2009). Respiration modulates BOLD signal across the entire brain, but that modulation is stronger in somatosensory, motor, and visual cortices than other brain regions (Birn et al., 2006; Wise et al., 2004). Compared to other areas, these regions show stronger correlations both with global signal (Fox et al., 2009) and with individual differences in head motion (Pujol et al., 2014; Yan et al., 2013a). These patterns could indicate that changes in respiration are frequently accompanied by head motion and that these respiration changes may ultimately be a core driver of global artifact in the BOLD signal. This hypothesis should be tested directly in future work.

Disadvantages of unmitigated global artifact

Concerns have been raised regarding global signal regression (e.g., Murphy et al., 2009; Saad et al., 2012; Schölvinck et al., 2010), which may also apply to MGTR. However, we argue that a major, under-addressed concern in the literature is that unmitigated motion-correlated artifact can be mistakenly attributed to meaningful individual or group differences. Researchers are rightly concerned about reducing sensitivity to individual and group differences by inadvertently discarding signal. Nonetheless, we argue that is critical to fully address motion-correlated artifact when researching individual and group differences that covary with head motion.

If head motion is correlated with one's variable of interest, any motion-correlated artifact that is retained can be mistakenly attributed to that variable of interest. Denoising strategies that are too lenient could result in features similar to motion-correlated artifact – such as distance-dependent correlations and globally-increased correlations – being attributed to a wide variety of clinical, developmental, and psychological group differences. Unfortunately, the publication bias in scientific literature (Franco et al., 2014) may make it relatively easy to report significant correlations resulting from motion-correlated artifact, but harder to refute such findings with correlations that are not significant after denoising. Therefore, we lean toward being more conservative with denoising to avoid contaminating the literature with artifactual findings.

In our opinion, time series denoising methods such as those investigated here are strongly preferred to leaving behind unmitigated motion artifact in rfMRI data. In the current study, the denoising methods were chosen to target and remove specific aspects of time series variance that have been linked to artifact, previously in the

literature (Birn et al., 2006; Friston et al., 1996; Wise et al., 2004), and empirically in the data (Power et al., 2014; Salimi-Khorshidi et al., 2014). Importantly, if rsFC estimates no longer correlate with individual and group differences after these time series denoising methods, it indicates that those variables only related to aspects of the time series that were removed by the denoising methods. If individual or group differences resulted entirely from aspects of the time series previously linked to artifact in the literature, it leads to substantial doubt that those differences might be neural in origin.

To adequately address global artifact while avoiding the drawbacks associated with global signal regression or MGTR, additional research is needed to identify denoising strategies that eliminate global artifact related to head motion and physiological processes. For example, CompCor (Behzadi et al., 2007; Chai et al., 2012) uses white matter and cerebrospinal fluid signal as confound regressors to address motion and physiological artifact without removing neural signal or inducing anti-correlations. However, Muschelli and colleagues (2014 Supplemental Figure 1) found increased correlations between FD and rsFC estimates across the brain after using CompCor, suggesting residual global artifact confounded with individual differences in head motion. Numerous other approaches (c.f., Yan et al., 2013c for examples) exist where participant-level motion estimates are treated as covariates in group-level and individual difference analyses. These approaches may reduce the influence of global artifact on those analyses. However, because these approaches regress out variance from the rsFC estimates rather than the time series, they may be less capable of separating motion-correlated artifact from meaningful individual differences confounded with motion.

After denoising HCP data with FIX+MGTR, we still observed a greater number of motion-group differences than expected by chance. It is possible that these motion-group differences reflect differences between the high- and low-motion participants in neural activity related to factors that might influence head motion, such as alertness, anxiety, cognition, etc. We believe that a comparison of within-participants motion effects versus between-participants motion effects may help to resolve this question. However, it is critical that future studies carefully equate the degree of head motion in within-participant with the between-participant analyses to which they are being compared.

Evaluation of Denoising Strategies To Address Motion-Correlated Artifact in Resting State fMRI Data from the Human Connectome Project (doi: 10.1089/brain.2016.0435)
This paper has been peer-reviewed and accepted for publication, but has yet to undergo copyediting and proof correction. The final published version may differ from this proof.

Brain Connectivity

Conclusion

Resting state fMRI data with high spatial and temporal resolution are available to the public from The Human Connectome Project (http://humanconnectome.org). Although cutting-edge technological advances have led to many improvements, HCP rfMRI data still are affected by artifact correlated with head motion and other physiological effects. An evaluation of artifactual changes in BOLD signal intensity suggests the presence of spatially-specific and global artifacts correlated with head motion. Several denoising techniques – including FIX-ICA denoising, motion regression, and censoring high-motion time points – primarily address spatially-specific artifact. However, these strategies leave substantial differences between rsFC estimates from high- and low-motion individuals. In contrast, MGTR primarily addresses global artifact, and substantially reduces rsFC differences between high- and low-motion individuals. Consequently, a combination of denoising strategies that captures both spatially-specific and global aspects of motion-correlated artifact will be necessary for productive analysis of HCP rfMRI data.

Acknowledgments

Data were provided by the Human Connectome Project, WU-Minn Consortium (Principal Investigators: David Van Essen and Kamil Ugurbil; 1U54MH091657) funded by the 16 NIH Institutes and Centers that support the NIH Blueprint for Neuroscience Research; and by the McDonnell Center for Systems Neuroscience at Washington University. We would like to thank A. M. Winkler, T. E. Nichols, and M. J. Strube for suggestions regarding valid methods for statistical inference. We would also like to thank Matt Glasser and David Van Essen for important perspectives and thoughts on this work. While we do not always agree on approaches and interpretations, their insights have provided valuable feedback on the work presented here. Finally, we thank the anonymous reviewers for their insightful comments and suggestions on an earlier version of the manuscript.

Disclosure Statement

No competing financial interests exist.

Brain Connectivity
Evaluation of Denoising Strategies To Address Motion-Correlated Artifact in Resting State fMRI Data from the Human Connectome Project (doi: 10.1089/brain.2016.0435)
This paper has been peer-reviewed and accepted for publication, but has yet to undergo copyediting and proof correction. The final published version may differ from this proof.

References

Behzadi, Y., Restom, K., Liau, J., Liu, T.T., 2007. A component based noise correction method (CompCor) for BOLD and perfusion based fMRI. NeuroImage 37, 90–101. doi:10.1016/j.neuroimage.2007.04.042

Birn, R.M., Diamond, J.B., Smith, M.A., Bandettini, P.A., 2006. Separating respiratory-variation-related fluctuations from neuronal-activity-related fluctuations in fMRI. NeuroImage 31, 1536–1548. doi:10.1016/j.neuroimage.2006.02.048

Birn, R.M., Smith, M.A., Jones, T.B., Bandettini, P.A., 2008. The respiration response function: the temporal dynamics of fMRI signal fluctuations related to changes in respiration. NeuroImage 40, 644–654. doi:10.1016/j.neuroimage.2007.11.059

Carp, J., 2013. Optimizing the order of operations for movement scrubbing: Comment on Power et al. NeuroImage 76, 436–438. doi:10.1016/j.neuroimage.2011.12.061

Chai, X.J., Castañón, A.N., Öngür, D., Whitfield-Gabrieli, S., 2012. Anticorrelations in resting state networks without global signal regression. NeuroImage 59, 1420–1428. doi:10.1016/j.neuroimage.2011.08.048

Chang, C., Glover, G.H., 2009. Relationship between respiration, end-tidal CO2, and BOLD signals in resting-state fMRI. NeuroImage 47, 1381–1393. doi:10.1016/j.neuroimage.2009.04.048

Epstein, J.N., Casey, B.J., Tonev, S.T., Davidson, M., Reiss, A.L., Garrett, A., Hinshaw, S.P., Greenhill, L.L., Vitolo, A., Kotler, L.A., Jarrett, M.A., Spicer, J., 2007. Assessment and prevention of head motion during imaging of patients with attention deficit hyperactivity disorder. Psychiatry research 155, 75–82. doi:10.1016/j.pscychresns.2006.12.009

Feinberg, D.A., Moeller, S., Smith, S.M., Auerbach, E., Ramanna, S., Glasser, M.F., Miller, K.L., Ugurbil, K., Yacoub, E., 2010. Multiplexed echo planar imaging for sub-second whole brain FMRI and fast diffusion imaging. PLoS ONE 5, e15710. doi:10.1371/journal.pone.0015710

Fox, M.D., Zhang, D., Snyder, A.Z., Raichle, M.E., 2009. The global signal and observed anticorrelated resting state brain networks. J Neurophysiol 101, 3270–3283. doi:10.1152/jn.90777.2008

Franco, A., Malhotra, N., Simonovits, G., 2014. Social science. Publication bias in the social sciences: unlocking the file drawer. Science 345, 1502–1505. doi:10.1126/science.1255484

Friston, K.J., Williams, S., Howard, R., Frackowiak, R.S., Turner, R., 1996. Movement-related effects in fMRI time-series. Magn Reson Med 35, 346–355.

Glasser, M.F., Sotiropoulos, S.N., Wilson, J.A., Coalson, T.S., Fischl, B., Andersson, J.L., Xu, J., Jbabdi, S., Webster, M., Polimeni, J.R., Van Essen, D.C., Jenkinson, M., Consortium, W.-M.H., 2013. The minimal preprocessing pipelines for the Human Connectome Project. NeuroImage 80, 105–124. doi:10.1016/j.neuroimage.2013.04.127

Gordon, E.M., Laumann, T.O., Adeyemo, B., Huckins, J.F., Kelley, W.M., Petersen, S.E., 2014. Generation and Evaluation of a Cortical Area Parcellation from Resting-State Correlations. Cereb Cortex 26, 288–303. doi:10.1093/cercor/bhu239

Jo, H.J., Gotts, S.J., Reynolds, R.C., Bandettini, P.A., Martin, A., Cox, R.W., Saad, Z.S., 2013. Effective Preprocessing Procedures Virtually Eliminate Distance-Dependent Motion Artifacts in Resting State FMRI. J Appl Math 2013, 1–9.

doi:10.1155/2013/935154

Kong, X.-Z., Zhen, Z., Li, X., Lu, H.-H., Wang, R., Liu, L., He, Y., Zang, Y., Liu, J., 2014. Individual differences in impulsivity predict head motion during magnetic resonance imaging. PLoS ONE 9, e104989. doi:10.1371/journal.pone.0104989

Mamah, D., Barch, D.M., Repovš, G., 2013. Resting state functional connectivity of five neural networks in bipolar disorder and schizophrenia. J Affect Disord 150, 601–609. doi:10.1016/j.jad.2013.01.051

Murphy, K., Birn, R.M., Handwerker, D.A., Jones, T.B., Bandettini, P.A., 2009. The impact of global signal regression on resting state correlations: are anti-correlated networks introduced? NeuroImage 44, 893–905. doi:10.1016/j.neuroimage.2008.09.036

Muschelli, J., Nebel, M.B., Caffo, B.S., Barber, A.D., Pekar, J.J., Mostofsky, S.H., 2014. Reduction of motion-related artifacts in resting state fMRI using aCompCor. NeuroImage 96, 22–35. doi:10.1016/j.neuroimage.2014.03.028

Power, J.D., Barnes, K.A., Snyder, A.Z., Schlaggar, B.L., Petersen, S.E., 2012. Spurious but systematic correlations in functional connectivity MRI networks arise from subject motion. NeuroImage 59, 2142–2154. doi:10.1016/j.neuroimage.2011.10.018

Power, J.D., Mitra, A., Laumann, T.O., Snyder, A.Z., Schlaggar, B.L., Petersen, S.E., 2014. Methods to detect, characterize, and remove motion artifact in resting state fMRI. NeuroImage 84, 320–341. doi:10.1016/j.neuroimage.2013.08.048

Power, J.D., Schlaggar, B.L., Petersen, S.E., 2015. Recent progress and outstanding issues in motion correction in resting state fMRI. NeuroImage 105C, 536–551. doi:10.1016/j.neuroimage.2014.10.044

Pujol, J., Macià, D., Blanco-Hinojo, L., Martínez-Vilavella, G., Sunyer, J., la Torre, de, R., Caixàs, A., Martín-Santos, R., Deus, J., Harrison, B.J., 2014. Does motion-related brain functional connectivity reflect both artifacts and genuine neural activity? NeuroImage 101, 87–95. doi:10.1016/j.neuroimage.2014.06.065

Saad, Z.S., Gotts, S.J., Murphy, K., Chen, G., Jo, H.J., Martin, A., Cox, R.W., 2012. Trouble at rest: how correlation patterns and group differences become distorted after global signal regression. Brain Connect 2, 25–32. doi:10.1089/brain.2012.0080

Salimi-Khorshidi, G., Douaud, G., Beckmann, C.F., Glasser, M.F., Griffanti, L., Smith, S.M., 2014. Automatic denoising of functional MRI data: Combining independent component analysis and hierarchical fusion of classifiers. NeuroImage 90, 449–468. doi:10.1016/j.neuroimage.2013.11.046

Satterthwaite, T.D., Elliott, M.A., Gerraty, R.T., Ruparel, K., Loughead, J., Calkins, M.E., Eickhoff, S.B., Hakonarson, H., Gur, R.C., Gur, R.E., Wolf, D.H., 2013. An improved framework for confound regression and filtering for control of motion artifact in the preprocessing of resting-state functional connectivity data. NeuroImage 64, 240–256. doi:10.1016/j.neuroimage.2012.08.052

Satterthwaite, T.D., Wolf, D.H., Loughead, J., Ruparel, K., Elliott, M.A., Hakonarson, H., Gur, R.C., Gur, R.E., 2012. Impact of in-scanner head motion on multiple measures of functional connectivity: relevance for studies of neurodevelopment in youth. NeuroImage 60, 623–632. doi:10.1016/j.neuroimage.2011.12.063

Schölvinck, M.L., Maier, A., Ye, F.Q., Duyn, J.H., Leopold, D.A., 2010. Neural basis of global resting-state fMRI activity. Proc. Natl. Acad. Sci. U.S.A. 107, 10238–10243.

Brain Connectivity
Evaluation of Denoising Strategies To Address Motion-Correlated Artifact in Resting State fMRI Data from the Human Connectome Project (doi: 10.1089/brain.2016.0435)
This paper has been peer-reviewed and accepted for publication, but has yet to undergo copyediting and proof correction. The final published version may differ from this proof.

doi:10.1073/pnas.0913110107

Smith, S.M., Beckmann, C.F., Andersson, J., Auerbach, E.J., Bijsterbosch, J., Douaud, G., Duff, E., Feinberg, D.A., Griffanti, L., Harms, M.P., Kelly, M., Laumann, T., Miller, K.L., Moeller, S., Petersen, S., Power, J., Salimi-Khorshidi, G., Snyder, A.Z., Vu, A.T., Woolrich, M.W., Xu, J., Yacoub, E., Ugurbil, K., Van Essen, D.C., Glasser, M.F., Consortium, W.-M.H., 2013. Resting-state fMRI in the Human Connectome Project. NeuroImage 80, 144–168. doi:10.1016/j.neuroimage.2013.05.039

Smith, S.M., Miller, K.L., Moeller, S., Xu, J., Auerbach, E.J., Woolrich, M.W., Beckmann, C.F., Jenkinson, M., Andersson, J., Glasser, M.F., Van Essen, D.C., Feinberg, D.A., Yacoub, E.S., Ugurbil, K., 2012. Temporally-independent functional modes of spontaneous brain activity. Proc. Natl. Acad. Sci. U.S.A. 109, 3131–3136. doi:10.1073/pnas.1121329109

Ugurbil, K., Xu, J., Auerbach, E.J., Moeller, S., Vu, A.T., Duarte-Carvajalino, J.M., Lenglet, C., Wu, X., Schmitter, S., Van de Moortele, P.-F., Strupp, J., Sapiro, G., De Martino, F., Wang, D., Harel, N., Garwood, M., Chen, L., Feinberg, D.A., Smith, S.M., Miller, K.L., Sotiropoulos, S.N., Jbabdi, S., Andersson, J.L.R., Behrens, T.E.J., Glasser, M.F., Van Essen, D.C., Yacoub, E., WU-Minn HCP Consortium, 2013. Pushing spatial and temporal resolution for functional and diffusion MRI in the Human Connectome Project. NeuroImage 80, 80–104. doi:10.1016/j.neuroimage.2013.05.012

Van Dijk, K.R.A., Sabuncu, M.R., Buckner, R.L., 2012. The influence of head motion on intrinsic functional connectivity MRI. NeuroImage 59, 431–438. doi:10.1016/j.neuroimage.2011.07.044

Van Essen, D.C., Smith, S.M., Barch, D.M., Behrens, T.E.J., Yacoub, E., Ugurbil, K., Consortium, W.-M.H., 2013. The WU-Minn Human Connectome Project: an overview. NeuroImage 80, 62–79. doi:10.1016/j.neuroimage.2013.05.041

Wise, R.G., Ide, K., Poulin, M.J., Tracey, I., 2004. Resting fluctuations in arterial carbon dioxide induce significant low frequency variations in BOLD signal. NeuroImage 21, 1652–1664. doi:10.1016/j.neuroimage.2003.11.025

Yan, C.-G., Cheung, B., Kelly, C., Colcombe, S., Craddock, R.C., Di Martino, A., Li, Q., Zuo, X.-N., Castellanos, F.X., Milham, M.P., 2013a. A comprehensive assessment of regional variation in the impact of head micromovements on functional connectomics. NeuroImage 76, 183–201. doi:10.1016/j.neuroimage.2013.03.004

Yan, C.-G., Craddock, R.C., He, Y., Milham, M.P., 2013b. Addressing head motion dependencies for small-world topologies in functional connectomics. Front Hum Neurosci 7, 910. doi:10.3389/fnhum.2013.00910

Yan, C.-G., Craddock, R.C., Zuo, X.-N., Zang, Y.-F., Milham, M.P., 2013c. Standardizing the intrinsic brain: Towards robust measurement of inter-individual variation in 1000 functional connectomes. NeuroImage 80, 246–262. doi:10.1016/j.neuroimage.2013.04.081

Brain Connectivity
Evaluation of Denoising Strategies To Address Motion-Correlated Artifact in Resting State fMRI Data from the Human Connectome Project (doi: 10.1089/brain.2016.0435)
This paper has been peer-reviewed and accepted for publication, but has yet to undergo copyediting and proof correction. The final published version may differ from this proof.

Figure Captions

	Motion-group		
	Low-motion	Medium-motion	High-motion
Age:	mean = 29.43 sd = 3.62 min = 22 max = 36	mean = 28.92 sd = 3.74 min = 22 max = 36	mean = 28.98 sd = 3.31 min = 23 max = 35
Gender:	26 men 35 women	26 men 35 women	26 men 35 women
Race: Asian/Hawaiian/Pacific Is. Black or African Am. More than one Unknown or Not Reported White	 1 14 0 2 44	 2 12 1 1 45	 2 15 1 0 43
Ethnicity: Hispanic/Latino Not Hispanic/Latino	 8 53	 9 52	 4 57
Education:	mean = 15.082 sd = 1.9519 min = 11 max = 17	mean = 14.750 sd = 1.7527 min = 11 max = 17	mean = 14.550 sd = 1.6917 min = 12 max = 17
Proportion of Time Points Censored:	mean = 0.1602 sd = 0.0274 min = 0.0792 max = 0.1992	mean = 0.2333 sd = 0.0210 min = 0.2000 max = 0.2650	mean = 0.3384 sd = 0.0715 min = 0.2658 max = 0.6517
Mean FD:	mean = 0.1187 sd = 0. 0217 min = 0.0800 max = 0.1800	mean = 0.1460 sd = 0.0340 min = 0.0800 max = 0.2100	mean = 0.2157 sd = 0.0727 min = 0.1000 max = 0.5000

Table 1:

Demographic and head motion information broken down by motion group. Head motion, measured by mean FD or proportion of time points censored, differs between groups. However, there are no statistically significant differences among groups in age, gender, race, or ethnicity.

Table 2

*** p<.001 ** p<.01 * p<.05 Denoising Strategy	MPP		FIX		Change due to FIX	
	Mean	Slope	Mean	Slope	Mean	Slope
Before MGTR	-6.659×10^{-4}	5.677×10^{-3} ***	-4.204×10^{-3} ***	3.450×10^{-3} ***	-3.538×10^{-3}	-2.226×10^{-3}
After MGTR	-8.820×10^{-4} ***	5.683×10^{-3} ***	-2.086×10^{-4} *	2.896×10^{-3} ***	6.734×10^{-4} **	-2.787×10^{-3} **
Change due to MGTR	-2.161×10^{-4}	6.694×10^{-6}	3.995×10^{-3} ***	-5.538×10^{-4}		

Table 2:

Means and slopes of the ΔR plots as estimated using a general linear model. Differences between denoising strategies were determined by computing the difference in ΔR values for those strategies. Slopes are expressed as change in ΔR per 100 mm, roughly reflecting the difference between average short-distance and long-distance connections.

Table 3

*** p<.001 ** p<.01 * p<.05 Denoising Strategy	MPP		FIX		Change due to FIX	
	Mean	Slope	Mean	Slope	Mean	Slope
Before MGTR	0.3272 ***	-0.0549 *	0.1940 ***	-0.0450 **	-0.1332 **	0.0099
After MGTR	0.0296 ***	-0.0731 ***	0.0084 *	-0.0246	-0.0212 ***	0.0485 **
Change due to MGTR	-0.2975 ***	-0.0182	-0.1856 ***	0.0205 *		

Table 3:

Relationship of head motion ("QC") with the mean and slope of the rsFC-distance relationship. See Methods for more detail regardin how these relationships were computed. Slopes are expressed as change in QC-rsFC relationship per 100 mm, roughly reflecting the difference between average short-distance and long-distance connections.

Table 4

*** p<.001 ** p<.01 * p<.05	Distance Bin	Uncensored			Censored		
Denoising Strategy		Low vs. High	Med vs. High	Low vs. Med	Low vs. High	Med vs. High	Low vs. Med
MPP	All	22.02%***	0.13%**	0.04%*	12.27%***	0.11%*	0.04%*
	Short	23.91%***	0.23%**	0.05%	13.90%***	0.17%*	0.04%
	Medium	21.35%***	0.09%**	0.04%	11.55%***	0.08%*	0.05%
	Long	21.23%***	0.09%	0.04%	12.21%***	0.11%	0.03%
FIX	All	14.23%***	0.19%*	0.04%	12.07%***	0.12%*	0.08%*
	Short	16.77%***	0.24%**	0.04%	14.00%***	0.11%*	0.06%
	Medium	14.20%***	0.19%*	0.03%	12.03%***	0.13%*	0.09%*
	Long	8.64%***	0.14%	0.05%	7.98%***	0.08%	0.08%
MPP + MGTR	All	0.44%***	0.03%**	0.01%	0.20%***	0.02%	0.03%
	Short	0.90%***	0.04%	0.01%	0.28%**	0.02%	0.03%
	Medium	0.49%***	0.03%	0.01%	0.16%**	0.01%	0.03%
	Long	0.51%**	0.01%	0.01%	0.26%	0.01%	0.03%
FIX + MGTR	All	0.38%***	0.05%*	0.02%	0.28%***	0.04%	0.02%
	Short	0.40%***	0.03%	0.01%	0.27%**	0.03%	0.01%
	Medium	0.36%***	0.06%*	0.03%	0.28%***	0.05%*	0.03%
	Long	0.46%***	0.04%	0.01%	0.34%***	0.00%	0.01%

Table 4:

Percentage of connections showing motion-group differences at α = 0.000242. The percentage is reported for all connections, and separately for short-, medium-, and long-distance connections. The statistical significance is determined via permutation testing; significance level is noted with asterisks.

Figure 1

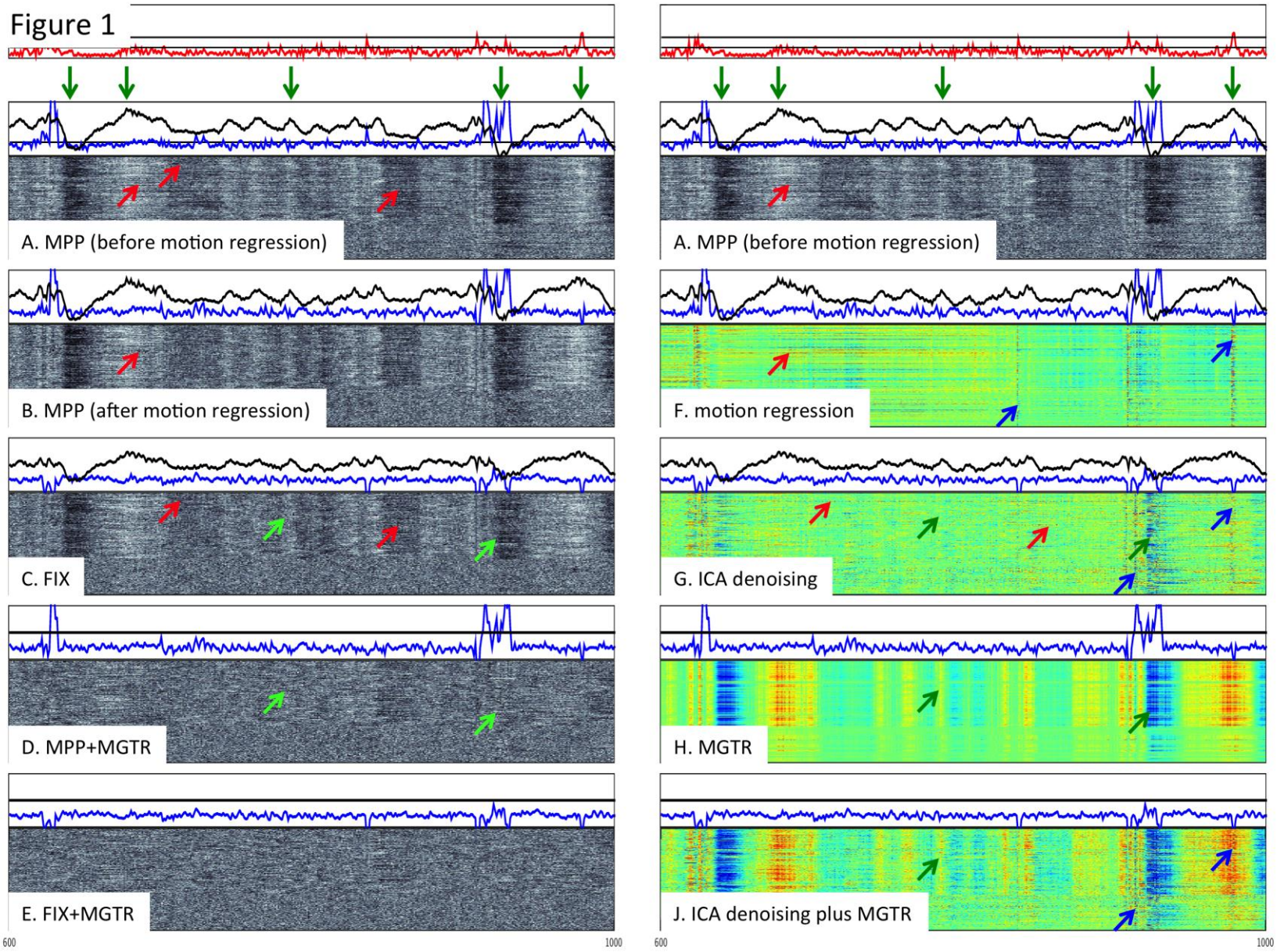

Figure 1:

Nature of BOLD fluctuations in HCP data, and aspects removed by each denoising stage: Five "residual grayordinate plots" (in grayscale on left) show rfMRI data after each denoising stage: A. MPP before motion regression, B. MPP after motion regression, C. FIX, D. MPP+MGTR, and E. FIX+MGTR. Four "difference grayordinate plots" (in color on right) show variance removed by specific denoising steps (estimated by subtracting the current preprocessing stage from a specified prior stage): F. motion regression (A – B); G. ICA denoising (B – C); H. MGTR (B – D); and J. ICA denoising plus MGTR (B – E). For each grayordinate plot, columns reflect time points and rows reflect grayordinates. Intensities are z-scored (across time, separately for each vertex), and range from -2 to +2.

The top panel on both sides shows FD (red), with horizontal lines marking FD = 0.2 mm (suggested as a censoring threshold by Power et al., 2014) and FD = 0.39mm (current study threshold for FD). MGT (black lines) and DVARS (blue lines) are derived from data after each denoising strategy. The horizontal line in Figure 1A corresponds to the DVARS censoring threshold of 4.9 arbitrary MR units. Green arrows indicate time periods displaying global artifact, which manifests as similar effects across space and occurs across most grayordinates. Spatially-specific artifacts, which manifest as dissimilar effects across space, are indicated by red arrows (instances that occurring at few grayordinates) and blue arrows (instances that occur across most grayordinates).

Figure 2

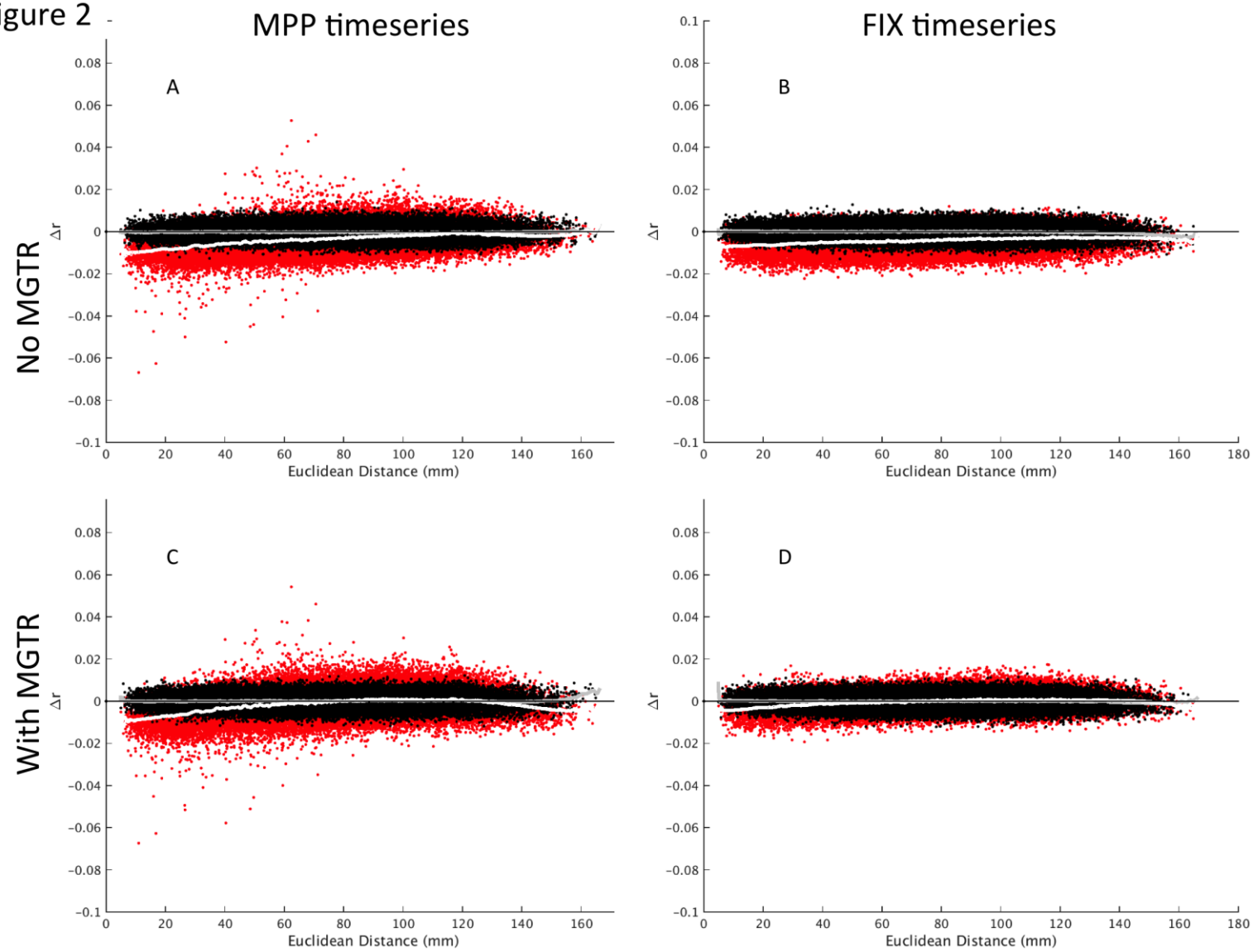

Delta-R plots: High motion group

Figure 2:

Censoring high-motion time points reveals spatially-specific and global shift artifact in ΔR plots: Red cloud (and white LOESS fit line) shows effects of censoring high-motion time points on rsFC estimates in the high-motion group, plotted as function of distance between parcels being correlated. Black cloud (and gray loess fit) shows positive control (censoring equal number of randomized time points). Range of ΔR (y-axis) from 0.1 to -0.1, following Power et al. (2014). Panels show effects of censoring on average rsFC estimates from high-motion group for A. MPP, B. FIX, C. MPP+MGTR, and D. FIX+MGTR time series data. Analogous plots for the low-motion group are in Supplemental Figure S3.

Figure 3

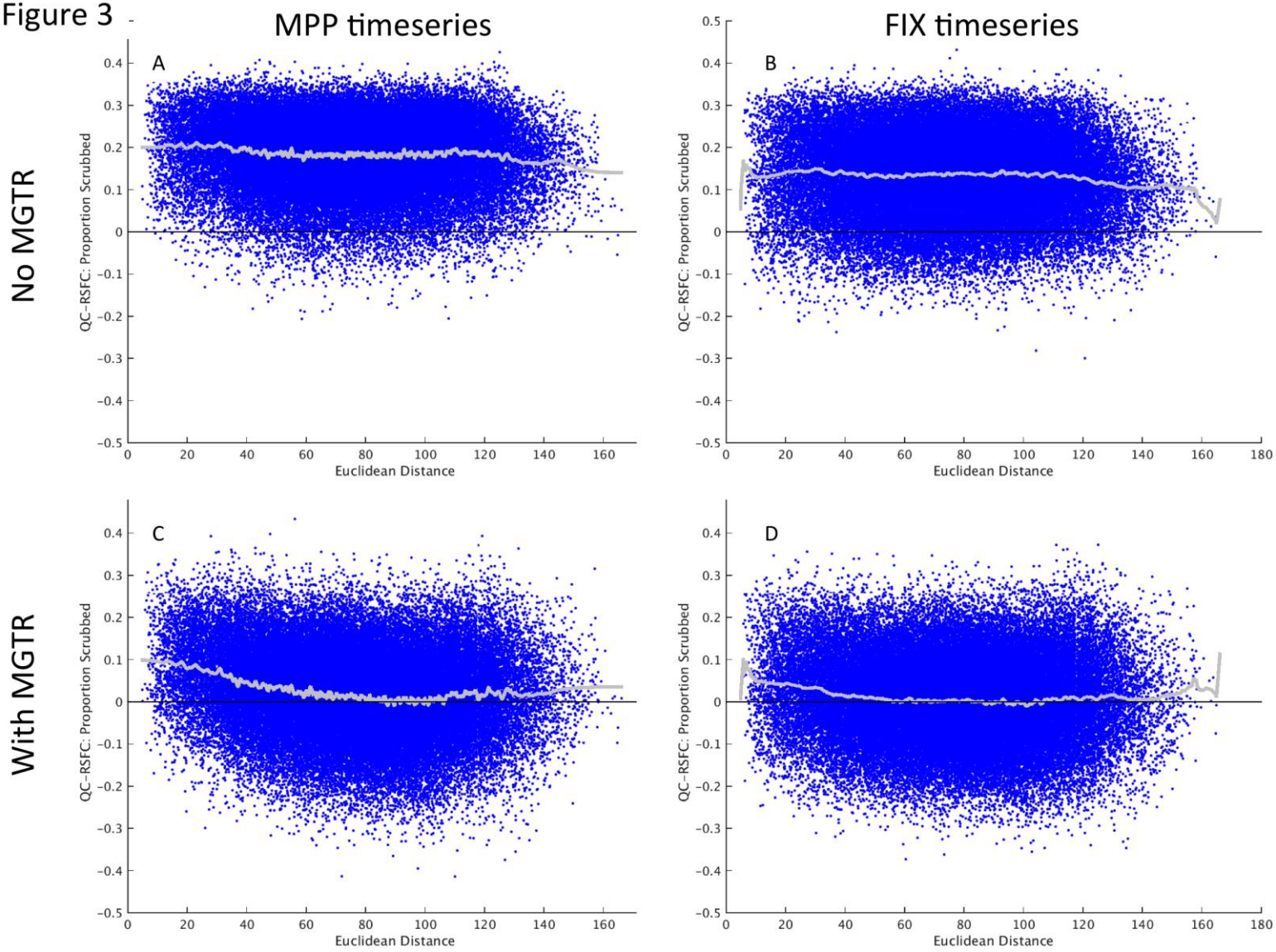

QC-rsFC plots: all participants (rsFC estimates after censoring)

Figure 3:

QC-rsFC plots show the correlation across participants between the rsFC estimates after censoring and degree of head motion (quantified by proportion of time points censored using the combined FD and DVARS criteria). The QC-rsFC relationship is plotted for each of the 61776 connections as a function of distance between parcels for A. MPP, B. FIX, C. MPP+MGTR, and D. FIX+MGTR time series data. Analogous plots for uncensored data are in Supplemental Figure S4.

Supplemental Materials:

Evaluation of Denoising Strategies To Address Motion-Correlated Artifact in Resting State fMRI Data from the Human Connectome Project

Gregory C. Burgess

Sridhar Kandala

Dan Nolan

Timothy O. Laumann

Jonathan D. Power

Babatunde Adeyemo

Michael P. Harms

Steven E. Petersen

Deanna M. Barch

HCP Minimal Preprocessing Procedures:

Structural and fMRI minimal preprocessing for HCP rfMRI data was identical to that described previously (Glasser et al., 2013), except that the HCP 500 subject release utilized the multimodal surface matching (MSM, Robinson et al., 2013; Smith et al., 2013) algorithm using FreeSurfer's sulcal depth measure ('sulc') to perform cortical inter-participant registration to the surface group-average template.

The fMRI time series images were processed in the fMRIVolume pipeline (Glasser et al., 2013) which concatenates a set of transformations to register the fMRI time series to MNI152 standard space (gradient- and field-inhomogeneity distortion corrections, rigid-body motion correction, two-step registration to T1w anatomical with FSL's FLIRT+BBR and freesurfer's BBRegister, nonlinear T1w-to-MNI registration) and applies them in a one-step spline resampling. Volume images were intensity normalized to a 4D global mean of 10,000.

Subsequently, in the fMRISurface pipeline, the standard space fMRIVolume time series was mapped to grayordinates. Voxels within the FreeSurfer cortical gray matter ribbon were mapped to the native cortical surface mesh, downsampled to the registered "32k_fs" mesh, and smoothed with a 2 mm FWHM Gaussian surface smoothing filter. The fMRI time series of subcortical gray matter voxels were assigned to FreeSurfer parcels using a parcel-constrained atlas smoothing/resampling process. The ultimate output was a CIFTI dense time series file containing the time series for cortical surface vertices from both hemispheres and the time series for subcortical voxels constrained to gray matter parcels.

HCP FIX-Denoising Procedures

Here, we detail the main steps of the FIX-ICA denoising pipeline, which factor into the additional preprocessing applied to the MPP data. The HCP FIX-ICA denoising pipeline has five main steps: 1) remove very slow, effectively linear, trends using a gentle high-pass temporal filter (cutoff=2000 s, as implemented by 'fslmaths'), 2) conduct spatial ICA analysis to decompose the volume time series data into independent spatial components, 3) separate those components into noise (artifact) and signal components using an automatic classifier trained on 100 scan runs from 25 HCP participants (17 women), 4) regress out the full variance associated with the 24 motion parameters, and 5) apply a "non-aggressive" regression of the noise component time series to remove noise variance that is orthogonal to signal components (Salimi-Khorshidi et al., 2014). FIX classifies noise components using volumetric maps as input, since the noise components may extend into white matter and CSF, which may provide useful information to help classify them into signal and noise (Salimi-Khorshidi et al., 2014). However, the time series of the noise components can be regressed from either volume or grayordinate data to yield FIX-denoised rfMRI data.

Selecting motion groups:

The tendency to produce head motion may be heritable (Couvy-Duchesne et al., 2014; Winkler et al., 2015)**. To avoid inflating statistical significance, we narrowed the participant list from 452 participants with four rfMRI scans to a group of 204 unrelated participants. For all analyses described below, we used only their complete "rfMRI_REST1_RL" scan (1200 time points; 14.4 minutes). We further split this subset of participants into three motion groups, ranked by the**

proportion of high-motion time points in their rfMRI scan (See "*Defining high-motion time points – FD and DVARS"* below).

Initially, each motion group had a different ratio of men to women (high-motion: 30M to 38F; medium-motion: 33M to 35F; low-motion: 26M to 42F). To avoid confounding gender with motion, we matched the gender ratio in all three groups by selecting within each motion-group 26 men and 35 women at random.

Defining high-motion time points – FD and DVARS:

FD (*F*ramewise *D*isplacement) reflects relative displacement of the head between adjacent time points, using the formula from Power and colleagues (2012). The backward difference of the rigid-body motion parameter time series provided estimates of displacement and rotation between time points. Rotations were converted to millimeter displacement on a 50mm radius sphere. The absolute values of the six displacement estimates were summed to provide the estimate of FD at each time point. DVARS (temporal *D*erivative, then RMS *VAR*iance over element*S*) was computed as the RMS intensity change between adjacent time points, using the formula from Smyser and colleagues (2010) by taking the backward difference of the MPP CIFTI dense time series, and computing the root mean square of that signal change across all grayordinates.

There are two notable differences in behavior of FD and DVARS in the HCP fMRI data compared to previously published examples. Figure S1 shows an example of FD and DVARS for one medium-motion participant across 400 time points (4.8 minutes). Additional examples of FD and DVARS can be seen at the top of Figure 1. First, periodic fluctuations in FD (Figure S1, red line) appear greater in HCP rfMRI data

Brain Connectivity
Evaluation of Denoising Strategies To Address Motion-Correlated Artifact in Resting State fMRI Data from the Human Connectome Project (doi: 10.1089/brain.2016.0435)
This paper has been peer-reviewed and accepted for publication, but has yet to undergo copyediting and proof correction. The final published version may differ from this proof.

compared to previously published data. These fluctuations may arise from physiologically-based movement, such as breathing or heart beats, being better sampled with faster acquisition. These increased fluctuations relate to higher mean FD, a larger proportion of time points being censored by a conservative FD threshold, and a smaller separation between abrupt motion "spikes" and the baseline "noise floor". In the HCP rfMRI data, DVARS appeared to separate large, transient changes from baseline noise levels (Figure S1, blue line) better than FD (Figure S1, red line). The additional variance in FD related to periodic fluctuations may have contributed to a lower correlation between FD and DVARS time series in the HCP rfMRI data (mean r=0.41 across participants) compared to previously published data (Power et al., 2014).

----------Insert Figure S1 about here----------

Second, median DVARS was observed to vary substantially from participant to participant, and correlates with participant head size (r=0.52). Median DVARS value will increase with thermal noise. Thermal noise is directly related to coil loading (Triantafyllou et al., 2005), which is impacted by head size. We median-centered the DVARS time series to remove the impact of baseline differences in thermal noise across participants, and focus on transient fluctuations in DVARS.

To overcome limitations with the individual motion measures, we combined censoring criterion based on FD or DVARS values. The overall degree of head motion within the scan was quantified as the proportion of time points that surpassed either the FD or DVARS criteria. **The censoring thresholds for FD and DVARS were chosen using the empirical rank procedure of Power and colleagues** (2014 Figure 11B; see also Figure S2)**. The empirical rank procedure helps to identify the amount of**

motion (i.e., FD or DVARS) corresponding to a large proportion of extreme correlations (e.g., empirical rank above 90th or 95th percentile). We visually inspected the grayordinate plots to ensure a rough correspondence in time between time points censored by the chosen thresholds and disturbances or extreme values in the grayordinate time series. For FD, this suggested a more liberal threshold (FD > 0.39 mm) than proposed by Power and colleagues (2014) to focus on faster, larger, punctate motion rather than discarding data with elevated FD from slower, periodic (e.g., physiologically-related) motion. For DVARS, this procedure suggested a censoring threshold greater than 4.9 arbitrary units[1] above the median DVARS for the scan.

Relating FD and DVARS

The combined censoring criterion was weighted more strongly toward censoring a time point based on DVARS (censoring ~25% of time points across all scans) than FD (censoring ~3% of time points across all scans). Despite the stronger weighting toward DVARS, the proportion of time points censored by the combined censoring criterion was strongly correlated with both mean FD (Spearman ρ=0.75) and the proportion of time points surpassing solely the FD criterion (Spearman ρ=0.74).

There was some concern about the increased reliance on DVARS over FD for assigning participants to motion groups. Because DVARS is derived from the difference in image intensity between successive time points, DVARS values could be affected by changes in global signal resulting from physiological processes or even neural global signal. If this were true, motion-group differences between groups ranked by our

[1] During preprocessing, HCP fMRI NIFTI volumes are normalized to a grand mean of 10000.

Brain Connectivity
Evaluation of Denoising Strategies To Address Motion-Correlated Artifact in Resting State fMRI Data from the Human Connectome Project (doi: 10.1089/brain.2016.0435)
This paper has been peer-reviewed and accepted for publication, but has yet to undergo copyediting and proof correction. The final published version may differ from this proof.

measure of head motion might be due instead to differences in global signal between successive time points due to physiological artifact or neural global signal. However, changes in image intensity due to neural activity are mediated by a slow response function (Boynton et al., 1996; Glover, 1999), as are aspects of BOLD signal related to respiration (Birn et al., 2008) and heart rate (Chang et al., 2009). These slow response functions will limit the potential changes in image intensity that occur between adjacent time points (especially with faster TR), and thereby limit the influence of these factors on DVARS values.

To verify that changes in the mean grayordinate time series between successive time points did not affect the ranking of participants into high- versus low-motion groups, we recomputed DVARS values after the influence of mean grayordinate time series was removed by regressing the mean grayordinate time series and backward derivative of the mean grayordinate time series from the MPP time series. DVARS and the mean grayordinate time series are mathematically related by the following equation: $DVARS^2 = dMGT^2 + sVar$, where dMGT is the backward difference of the mean grayordinate time series, and sVar is the variance of the backward difference signal over space. Therefore, DVARS values recomputed after regressing mean grayordinate time series and the backward derivative of the mean grayordinate time series are influenced solely by sVar. 84% of high-motion participants from the original motion-groups were still designated high-motion using the post-MGTR DVARS values, and 75% of low-motion participants from the original motion-groups were still designated low-motion using the post-MGTR DVARS values. More importantly, the number of differences between high- and low-motion groups observed in rsFC estimates derived from the MPP data was very

similar whether groups were ranked using our original criteria or using post-MGTR DVARS. This suggests that the influence of the mean grayordinate time series on DVARS values is very small, and that changes in mean grayordinate time series between successive time points are not driving the assignment of participants to high- versus low-motion groups in the current study.

Performing MGTR on FIX data:

We were concerned that the prior regression of 24 motion parameters and noise components from the FIX rfMRI data could cause the mean grayordinate time series from the original MPP data to poorly fit the FIX time series. Therefore, to perform MGTR on the FIX time series, we computed the mean grayordinate time series from the FIX-denoised time series and regressed it from the FIX rfMRI data.

Performing additional high pass temporal filtering:

Additional temporal frequency filtering was conducted after regressing confound time series (Carp, 2013)**. For each denoising strategy, the appropriate time series confounds were regressed (e.g., 24 motion regressor time series, unique variance in ICA noise components, mean grayordinate time series) before high-pass filtering with a second-order zero-phase Butterworth filter (threshold = 0.009 Hz). In analyses involving censoring, temporal frequency filtering was done after linear interpolation over high-motion time points.**

Grayordinate plots:

The order of grayordinate rows is described by Glasser and colleagues (2013), with roughly the top third reflecting left cortex, the middle third reflecting right cortex,

and the bottom third reflecting cerebellum and subcortical grayordinates. Grayordinates were automatically subsampled during plotting. This may make spatially-specific fluctuations more difficult to see in grayordinate plots, because they are spread across discontiguous rows and compressed during plotting.

Parcellated connectomes:

This parcellation of Gordon and colleagues (2014) consists of 333 surface-based parcels. Because this parcellation does not contain subcortical regions, we added 19 subcortical parcels (i.e., brainstem, plus left/right amygdala, hippocampus, accumbens, caudate, pallidum, putamen, thalamus, ventral diencephalon, and cerebellum) from the standard subcortical segmentation in 2mm MNI space contained in the group-average CIFTI atlas (Glasser et al., 2013), for a total of 352 parcels.

For subsequent analyses requiring distance between parcels, we computed the Euclidean distance between the estimated centers of the parcels in MNI coordinates. To estimate the center of subcortical parcels, we simply averaged the voxel coordinates in MNI space. To estimate the center of surface parcels, we averaged the X, Y, and Z coordinates within each parcel on the HCP Q1-Q6 average midthickness surface. Then, we utilized the “surface-closest-vertex” function in the Connectome Workbench wb_command utility to find the coordinate of the cortical vertex nearest to the computed average.

Establishing alpha level for testing motion-group differences

An alpha of 0.05 (uncorrected for multiple comparisons) would limit our ability to compare the efficacy of denoising methods in the presence of large motion-related artifacts. For example, if motion-related artifact inflated effects 20 times larger than chance under one strategy and 40 times larger than chance under another, we might expect both scenarios to show significant motion-group differences for every pairwise correlation. In contrast, a Bonferroni-corrected alpha resulting in a familywise error rate of 5% would limit our ability to compare denoising methods in the presence of small motion-related artifacts. For example, it would be possible to see only 1 significant motion-group difference under a denoising method that entirely eliminated motion-related artifact and a second method that inflated motion-group differences 20 times larger than chance.

Although a wide range of alpha values might have achieved these goals, we chose α = 0.000242, equivalent to 300 times the Bonferroni-corrected alpha of 5%. **(There were 61776 total possible pairwise correlations (ignoring directionality) among the 333 surface parcels** (Gordon et al., 2014) **and the 19 subcortical gray matter parcels** (Glasser et al., 2013)**.)** At this alpha level, we would expect roughly 15 significant tests under the null hypothesis that there were no motion-group differences. Both small effects (e.g., two times larger than chance) and very large effects (e.g., 4000 times larger than chance) should be detectable at this alpha level.

Brain Connectivity
Evaluation of Denoising Strategies To Address Motion-Correlated Artifact in Resting State fMRI Data from the Human Connectome Project (doi: 10.1089/brain.2016.0435)
This paper has been peer-reviewed and accepted for publication, but has yet to undergo copyediting and proof correction. The final published version may differ from this proof.

References

Birn, R.M., Smith, M.A., Jones, T.B., Bandettini, P.A., 2008. The respiration response function: the temporal dynamics of fMRI signal fluctuations related to changes in respiration. NeuroImage 40, 644–654. doi:10.1016/j.neuroimage.2007.11.059

Boynton, G.M., Engel, S.A., Glover, G.H., Heeger, D.J., 1996. Linear systems analysis of functional magnetic resonance imaging in human V1. Journal of neuroscience 16, 4207–4221.

Carp, J., 2013. Optimizing the order of operations for movement scrubbing: Comment on Power et al. NeuroImage 76, 436–438. doi:10.1016/j.neuroimage.2011.12.061

Chang, C., Cunningham, J.P., Glover, G.H., 2009. Influence of heart rate on the BOLD signal: the cardiac response function. NeuroImage 44, 857–869. doi:10.1016/j.neuroimage.2008.09.029

Couvy-Duchesne, B., Blokland, G.A.M., Hickie, I.B., Thompson, P.M., Martin, N.G., de Zubicaray, G.I., McMahon, K.L., Wright, M.J., 2014. Heritability of head motion during resting state functional MRI in 462 healthy twins. NeuroImage 102P2, 424–434. doi:10.1016/j.neuroimage.2014.08.010

Glasser, M.F., Sotiropoulos, S.N., Wilson, J.A., Coalson, T.S., Fischl, B., Andersson, J.L., Xu, J., Jbabdi, S., Webster, M., Polimeni, J.R., Van Essen, D.C., Jenkinson, M., Consortium, W.-M.H., 2013. The minimal preprocessing pipelines for the Human Connectome Project. NeuroImage 80, 105–124. doi:10.1016/j.neuroimage.2013.04.127

Glover, G.H., 1999. Deconvolution of impulse response in event-related BOLD fMRI. NeuroImage 9, 416–429.

Gordon, E.M., Laumann, T.O., Adeyemo, B., Huckins, J.F., Kelley, W.M., Petersen, S.E., 2014. Generation and Evaluation of a Cortical Area Parcellation from Resting-State Correlations. Cereb Cortex 26, 288–303. doi:10.1093/cercor/bhu239

Power, J.D., Barnes, K.A., Snyder, A.Z., Schlaggar, B.L., Petersen, S.E., 2012. Spurious but systematic correlations in functional connectivity MRI networks arise from subject motion. NeuroImage 59, 2142–2154. doi:10.1016/j.neuroimage.2011.10.018

Power, J.D., Mitra, A., Laumann, T.O., Snyder, A.Z., Schlaggar, B.L., Petersen, S.E., 2014. Methods to detect, characterize, and remove motion artifact in resting state fMRI. NeuroImage 84, 320–341. doi:10.1016/j.neuroimage.2013.08.048

Robinson, E.C., Jbabdi, S., Andersson, J., Smith, S.M., Glasser, M.F., Van Essen, D.C., Burgess, G., Harms, M.P., Barch, D.M., 2013. Multimodal surface matching: fast and generalisable cortical registration using discrete optimisation. Inf Process Med Imaging 23, 475–486.

Salimi-Khorshidi, G., Douaud, G., Beckmann, C.F., Glasser, M.F., Griffanti, L., Smith, S.M., 2014. Automatic denoising of functional MRI data: Combining independent component analysis and hierarchical fusion of classifiers. NeuroImage 90, 449–468. doi:10.1016/j.neuroimage.2013.11.046

Smith, S.M., Beckmann, C.F., Andersson, J., Auerbach, E.J., Bijsterbosch, J., Douaud, G., Duff, E., Feinberg, D.A., Griffanti, L., Harms, M.P., Kelly, M., Laumann, T., Miller,

K.L., Moeller, S., Petersen, S., Power, J., Salimi-Khorshidi, G., Snyder, A.Z., Vu, A.T., Woolrich, M.W., Xu, J., Yacoub, E., Ugurbil, K., Van Essen, D.C., Glasser, M.F., Consortium, W.-M.H., 2013. Resting-state fMRI in the Human Connectome Project. NeuroImage 80, 144–168. doi:10.1016/j.neuroimage.2013.05.039

Smyser, C.D., Inder, T.E., Shimony, J.S., Hill, J.E., Degnan, A.J., Snyder, A.Z., Neil, J.J., 2010. Longitudinal analysis of neural network development in preterm infants. Cereb Cortex 20, 2852–2862. doi:10.1093/cercor/bhq035

Triantafyllou, C., Hoge, R.D., Krueger, G., Wiggins, C.J., Potthast, A., Wiggins, G.C., Wald, L.L., 2005. Comparison of physiological noise at 1.5 T, 3 T and 7 T and optimization of fMRI acquisition parameters. NeuroImage 26, 243–250. doi:10.1016/j.neuroimage.2005.01.007

Winkler, A.M., Webster, M.A., Vidaurre, D., Nichols, T.E., Smith, S.M., 2015. Multi-level block permutation. NeuroImage 123, 253–268. doi:10.1016/j.neuroimage.2015.05.092

Table S1

*** p<.001 ** p<.01 * p<.05 Denoising Strategy	MPP		FIX		Change due to FIX	
	Mean	Slope	Mean	Slope	Mean	Slope
Before MGTR	1.320×10^{-3}	2.215×10^{-5} **	-2.780×10^{-3} ***	5.951×10^{-6} **	-4.190×10^{-3}	-1.620×10^{-3} *
After MGTR	-4.563×10^{-4} ***	2.185×10^{-5} ***	-9.670×10^{-5} ***	9.287×10^{-6} ***	3.596×10^{-4} ***	-1.256×10^{-3} ***
Change due to MGTR	-1.776×10^{-3}	-3.031×10^{-5}	2.776×10^{-3} ***	3.336×10^{-4} *		

Evaluation of Denoising Strategies To Address Motion-Correlated Artifact in Resting State fMRI Data from the Human Connectome Project (doi: 10.1089/brain.2016.0435)

Table S2

*** p<.001 ** p<.01 * p<.05 Denoising Strategy	MPP		FIX		Change due to FIX	
	Mean	Slope	Mean	Slope	Mean	Slope
Before MGTR	0.3144 ***	-0.0817 ***	0.1913 ***	-0.0609 ***	-0.1332 **	0.0209
After MGTR	0.0315 ***	-0.0958 ***	0.0085 *	-0.0327 *	-0.0212 ***	0.0631 ***
Change due to MGTR	-0.2975 ***	-0.0141	-0.1856 ***	0.0282 **		

Figure S1

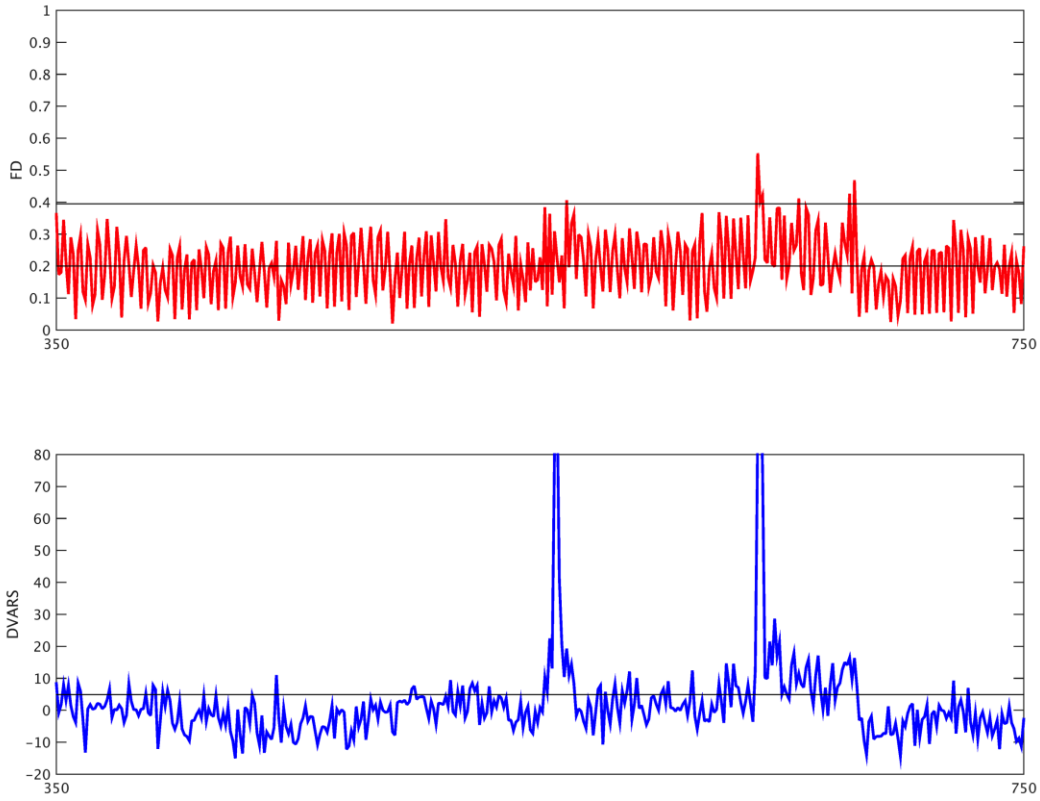

Compared to previously-published data, FD estimates from HCP fMRI data have less separation between high-motion "spikes" and the "noise floor", due in part to periodic fluctuations in FD across time. Example timeseries of FD (red) and DVARS (blue) from high-motion participant 159340, rfMRI_REST1_RL scan, time points 350 – 750. Horizontal lines on the FD plot correspond to FD = 0.2 mm (suggested as a censoring threshold by Power et al., 2014) and FD = 0.39 mm (FD threshold utilized for the current study). The horizontal line on the DVARS plot corresponds to DVARS = 4.9 (arbitrary MR units), the DVARS censoring threshold used for the current study.

Brain Connectivity
Evaluation of Denoising Strategies To Address Motion-Correlated Artifact in Resting State fMRI Data from the Human Connectome Project (doi: 10.1089/brain.2016.0435)
This paper has been peer-reviewed and accepted for publication, but has yet to undergo copyediting and proof correction. The final published version may differ from this proof.

Figure S2

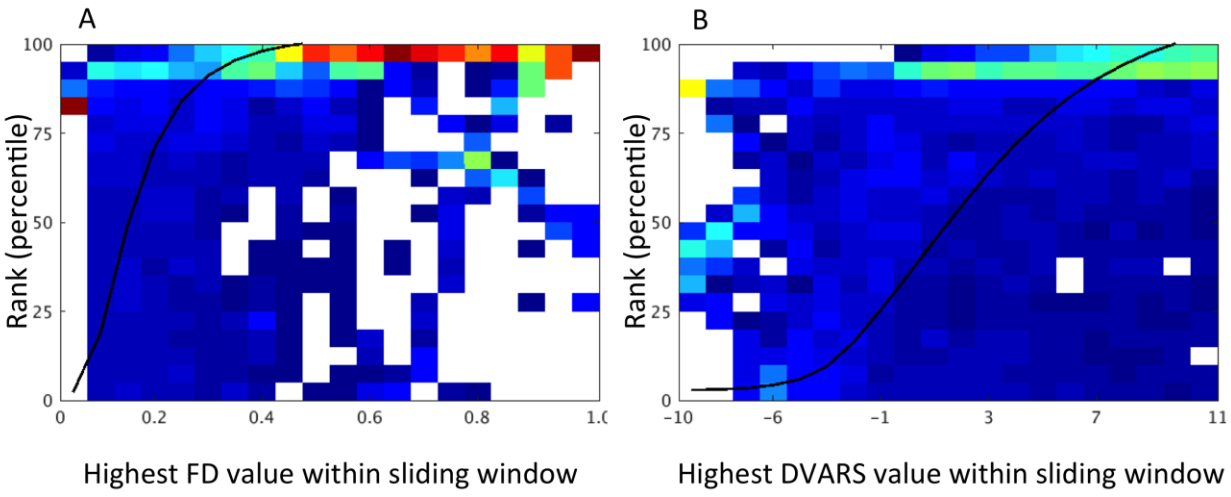

"Heat maps" (following the procedure used in Power et al. 2014, Figure 11B) demonstrate proportion of extreme correlations as a function of FD values (Panel A) or DVARS values (Panel B). X-axis reflects the FD (or DVARS) value of data within a sliding window. Y-axis reflects the empirical rank of the differences between correlations within the sliding window and correlations in the lowest FD (or DVARS) window. Color of box shows proportion of data at the sliding window that falls within that empirical rank. At each value of FD (or DVARS), roughly 5% of the data should fall by chance in each of the 20 empirical rank bins. Higher proportions of data falling in high empirical rank bins indicate more extreme differences in correlations for those FD (or DVARS) values compared to the lowest FD (or DVARS) window.

Figure S3

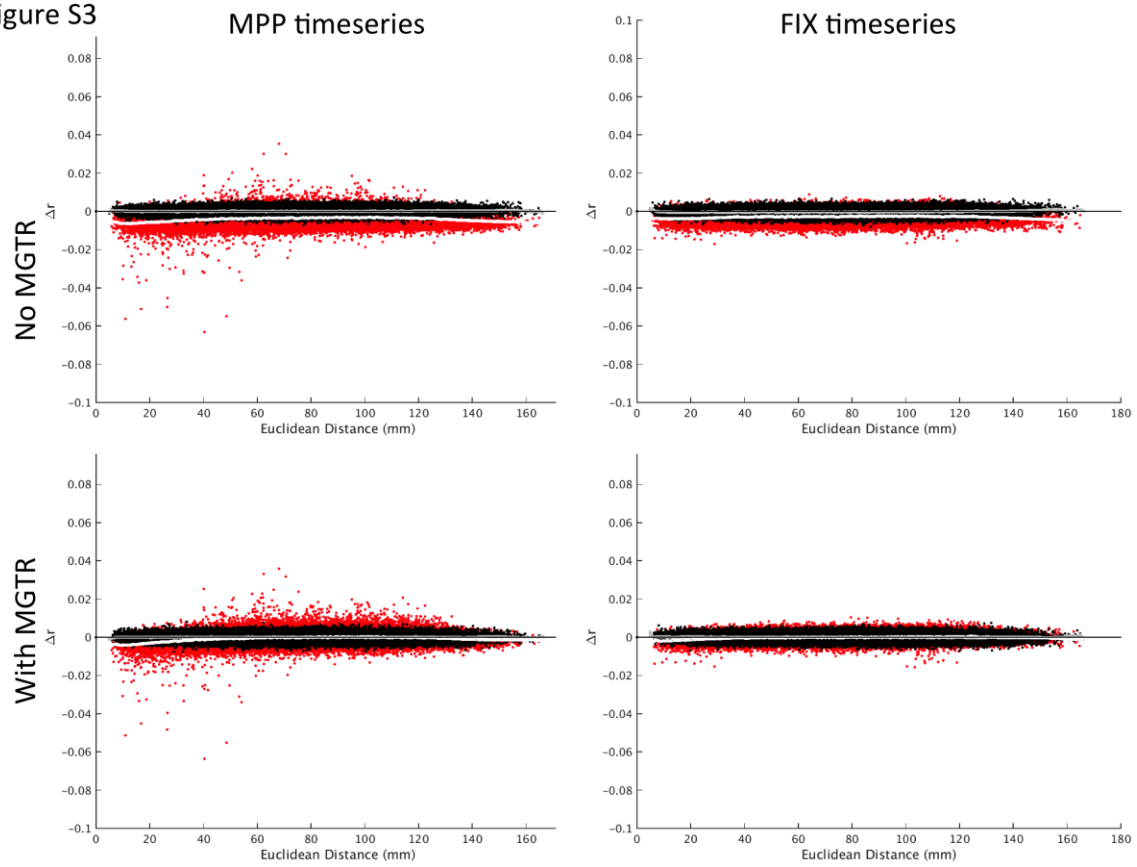

Delta-R plots: Low motion group (high pass filter)

Spatially-specific and global shift artifact are evident in ΔR plots for low-motion group after censoring high-motion time points: Red cloud (and white LOESS fit) shows effects of censoring high-motion time points on rsFC estimates, plotted as function of distance between parcels being correlated. Black cloud (and gray LOESS fit) shows positive control (censoring equal number of randomized time points). Range of ΔR (y-axis) from 0.1 to -0.1, following Power et al. (2014). Panels show effects of censoring on average rsFC estimates from low-motion group for A. MPP, B. FIX, C. MPP+MGTR, and D. FIX+MGTR timeseries data. Deviation from zero across all distances suggests global artifact, and increased deviation at short-distances compared to other distances suggests spatially-specific artifact.

Figure S4

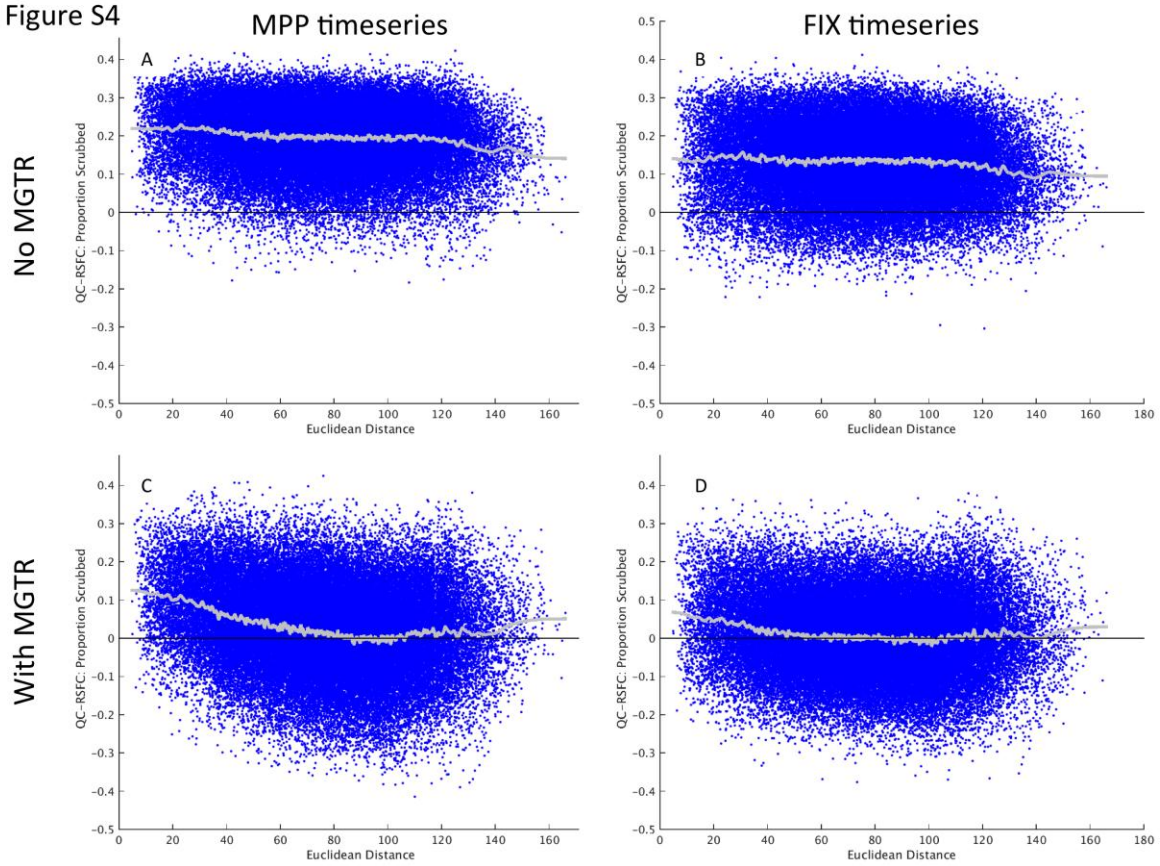

QC-rsFC plots: all participants (rsFC estimates before censoring)

QC-rsFC plots show the correlation across participants between the rsFC estimates before censoring and degree of head motion (quantified by proportion of time points exceeding the combined FD and DVARS criteria). The QC-rsFC relationship is plotted for each of the 61776 connections as a function of distance between parcels for A. MPP, B. FIX, C. MPP+MGTR, and D. FIX+MGTR timeseries data. Analogous plots for censored data are in Figure 3.